Mathematical Biosciences and Engineering

http://www.aimspress.com/journal/mbe

MBE, 20(9): 16279–16303.
DOI: 10.3934/mbe.2023727
Received: 02 May 2023
Revised: 20 July 2023
Accepted: 03 August 2023
Published: 14 August 2023

Research article

Research on robust fuzzy logic sliding mode control of Two-DOF intelligent underwater manipulators

Kangsen Huang*and Zimin Wang

International College, Wuhan University of Science and Technology, Wuhan 430065, China

* **Correspondence:** Email: KangsenHuang@163.com.

Abstract: This study investigates the independent motion control of a two-degree-of-freedom (Two-DOF) intelligent underwater manipulator. The dynamics model of two-DOF manipulators in an underwater environment is proposed by combining Lagrange's equation and Morison's empirical formulation. Disturbing factors such as water resistance moments, additional mass force moments and buoyancy forces on the intelligent underwater manipulator are calculated exactly. The influence of these factors on the trajectory tracking of the intelligent underwater manipulator is studied through simulation analysis. Based on the design of the sliding mode surface of the PID structure, a new Fuzzy-logic Sliding Mode Control (FSMC) algorithm is presented for the control error and control input chattering defects of traditional sliding mode control algorithm. The experimental simulation results show that the FSMC algorithm proposed in this study has a good effect in the elimination of tracking error and convergence speed, and has a great improvement in control accuracy and input stability.

Keywords: two-DOF intelligent underwater manipulator; dynamics model; PID; sliding mode control (SMC); fuzzy-logic sliding mode control (FSMC)

1. Introduction

Due to the over exploitation of terrestrial resources in recent years, depletion is now in full swing. The oceans, however, cover two-thirds of the earth's surface and are extremely rich in biological and mineral resources, so the process of marine development is accelerating in all countries of the world. In recent years, many scholars from all over the world have been involved in this research. Meng et al. concerned with the robust finite-time stability and stabilization of impulsive systems subject to hybrid disturbances that consists of external disturbances and hybrid impulses with time-varying jump maps [1]. An adaptive modified reaching law-based switch controller design was developed for robotic manipulator systems using the Disturbance Observer (DO) approach by Shao et al. [2]. To

suppress the flexible vibration of underwater manipulators, an Improved Sparrow Search Algorithm (ISSA) combining an elite strategy and a sine algorithm were proposed for the trajectory planning of underwater flexible manipulators [3]. To realize precise operation in underwater narrow spaces, the Fly Arm Underwater Vehicle Manipulator System (FAUVMS) was proposed [4]. Khadembashi et al. have studied beyond pull-in angle control of a dual axis torsional micro-actuator considering bending effects [5]. Jing et al. have proposed dynamic modeling and experimental analysis of an underwater glider in the ocean [6].

While only a single robot model has fewer realizable functions and is less practical, the robot body structure coupled with a self-contained manipulator model is becoming a hot research topic. Compared to conventional robots, robots working in underwater environments are characterized by non-linearity, hydrodynamic shocks and complex external disturbances, and their control faces the challenges of accurate dynamics modeling and high precision control of joint motion [7]. Recently, in order to realize the precise motion control of underwater hydraulic manipulator and make it suitable for underwater precision operations, an adaptive robust controller combined with backstepping strategy was proposed by Zhou et al. [8]. In connection with locating, trajectory planning and control of an underwater propeller cleaning manipulator, a solution for cleaning the propeller by the intelligent underwater manipulator was proposed by Long et al. [9]. Ema et al. investigated the comprehensive modeling and identification of the nonlinear joint dynamics of a collaborative robot. The proposed joint dynamics model and identification describe the most important dynamic characteristics of the robot joints, including nonlinear friction, nonlinear stiffness, hysteresis and motion errors [10]. A novel Non-singular Fast Terminal Sliding Mode (NFTSM) control strategy based on neural networks was proposed for n-linked robots with actuator dynamics [11]. Vimalesh Muralidharan et al. investigated the bit-shaped space and actuator space variables of the Lagrangian equations for the dynamics of a parallel robot [12]. Houssem Abdellatif et al. considered an open-loop sub-chain of the manipulator and derives its dynamics based on the Lagrangian form and a set of generalized coordinates and velocities. The determination of the stability of the method was an important task in the analysis of the system [13]. A robust non-linear PID fuzzy control method was proposed for the trajectory tracking control of an Autonomous Underwater Robotic Manipulator System (AURMS) for deep-sea intervention tasks [14]. Zeng et al. investigated the problem of the performance of the connection weight parameter on a regulatory PID Neural Network (PIDNN) in a complex control system [15]. Hamed Farivarnejad et al. have studied the control problem of a two-arm Underwater Vehicle-Manipulator System (UVMS) for a target manipulation task, and an explicit dynamics model of the UVMS was developed, where the additional mass, drag and buoyancy were considered as external forces and moments in the task space and incorporated into the model by means of a Jacobi matrix at their application points [16]. H. Farivarnejad and Saa Moosavian combined a task-first inverse kinematic redundancy solution method with fuzzy control techniques to achieve coordinated control of the robotic arm, using fuzzy control techniques for motion distribution between robot and manipulator and the handling of multiple auxiliary tasks [17]. Zhong et al. proposed a fuzzy adaptive PID fast terminal sliding mode controller for a redundancy degree robotic arm system with variable loads. The method achieved accurate tracking of the end-effector trajectory of the redundancy robotic arm and improved the robustness to model uncertainty and external disturbances when controlling the position of the redundancy robotic arm [18]. Next, Zhong et al. combined sliding mode control with fuzzy control and proposed an adaptive fuzzy sliding mode

control algorithm, which effectively solved the shortcomings such as jittering and achieved accurate and stable control of the robotic arm motion [19]. Lin developed a model-free self-organising fuzzy controller that can effectively control a 3-link manipulator. Simulation studies showed that the self-organising fuzzy controller outperformed a simple fuzzy logic controller in controlling the manipulator [20]. In addition, Amer et al. proposed an adaptive control scheme for robot-manipulators, namely adaptive fuzzy sliding mode control, and online adjustment by monitoring the fuzzy system. The effectiveness of the scheme was evaluated by comparing its performance with that of a conventional sliding-mode controller to assess the trajectory tracking problem of a 3-degree-of-freedom planar rigid robot manipulator with uncertainty [21]. Lu et al. proposed a robust Proportional-Integral (PI) controller with parameters that employ constraints to design a population extremum optimisation for a multi-area interconnected load frequency control problem, and the effectiveness of the proposed controller was verified by comparing other PI control methods with an optimized model predictive control method [22].

Esfahani et al. presented an improved Time-Delay Control (TDC) method for an underwater robot manipulator system, which used fuzzy rules to adaptively adjust the gain of the TDC and PID terms, and which not only had a higher trajectory tracking performance compared to a conventional sliding mode controller, but also had acceptable robustness in the presence of external disturbances and unknown forces/torques [23]. The Girona 500 AUV model, which is shown in Figure 1, which has a multi-joint manipulator attached to its base, and relies on its attached manipulator to perform all functions in the underwater environment [24–26]. For more manufacturing and control technology aspects of underwater manipulator, maybe we can refer to the innovative ideas in these literatures [27–29]. In these literatures, X. Xiao et al. introduced an automated method that allowed reorienting the part during the build using a five-axis machine. The reorientations still allow the part to be built using traditional planar deposition but without the use of supports.

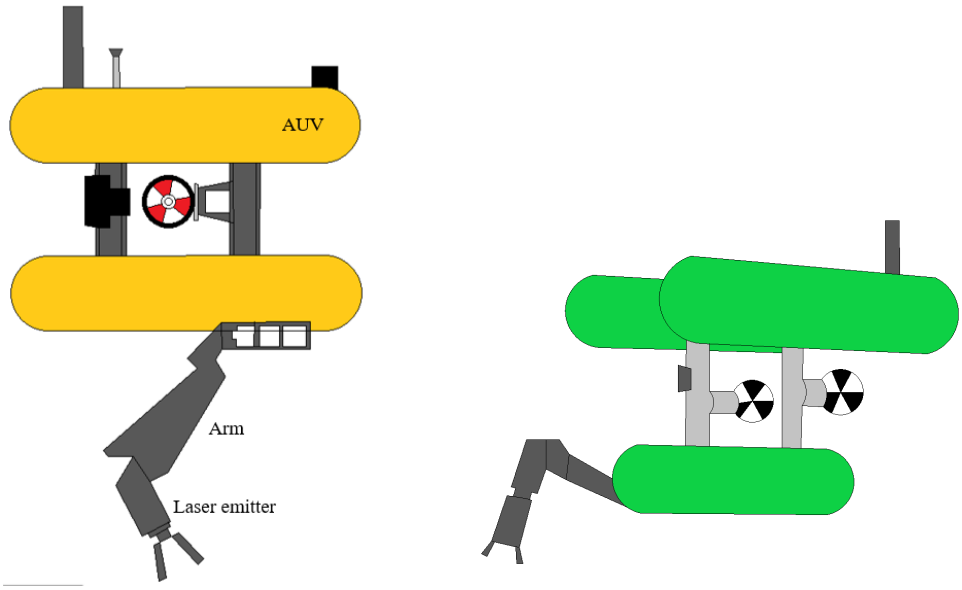

(a) AUV-I with multi-joint manipulator (b) AUV-II with multi-joint manipulator

Figure 1. Girona 500 AUV with multi-joint manipulator [26].

In addition, autonomous pilot is crucial in integrally promoting the autonomy of an Unmanned Surface Vehicle (USV). By organically bridging path planning and tracking, an autonomous pilot framework with waypoints generation, path smoothing and policy guidance of a USV in congested waters was established for the first time [30]. To exclusively suppress unuseful underwater noise feature and effectively avoid overenhancement, simultaneously, an underwater attentional generative adversarial network (UAGAN) was innovatively established [31]. A novel reinforcement learning-based optimal tracking control (RLOTC) scheme was established for an USV in the presence of complex unknowns. Simulation results and comprehensive comparisons on a prototype USV demonstrate remarkable effectiveness and superiority [32].

Taking the above research into consideration, we consider the motion of the connected manipulator when the underwater robot is in a horizontal hover state, and does not consider the interaction between the robot body and the manipulator. When the underwater robot is in a horizontal hovering state, considering the interference of multiple underwater factors, the dynamic equation of the two-degree-of-freedom manipulator is established in this study. A fuzzy sliding mode control combined with fuzzy logic control is proposed, which improves the error and stability of the traditional control method in the control process. The simulation results fully demonstrate the effectiveness and accuracy of the proposed improved control algorithm in the motion control of the manipulator.

The structure of this study is as follows. In Section 2, an accurate dynamics model of a two-degree-of-freedom manipulator in an underwater environment is developed. In Section 3, an improved fuzzy logic sliding mode control algorithm for the manipulator is proposed. In Section 4, the effects of three disturbance factors on the trajectory of the manipulator are first compared and studied by dynamic simulation. Then, the superiority of the proposed algorithm in terms of tracking accuracy and joint input stability is verified by comparing the simulation with the conventional sliding mode control algorithm. Finally, Section 5 summarizes the content and innovation in this study.

2. Dynamic modeling of Two-DOF intelligent underwater manipulator

It can be seen that there are multiple factors for the external disturbance of the intelligent underwater manipulator when moving in the underwater environment [19]. Assume that the water flow is stationary and the robot is fully immersed in the water. The connecting rods of the intelligent underwater manipulator are all cylinders, and at the same time, the center of gravity and the center of buoyancy of each component are coincident. Only the influence of the motion of the manipulator itself is concerned. According to the knowledge of fluid mechanics, when a single object moves in water, the force between the unit length of the object and the water can be described as shown in Eq (2.1):

$$\frac{dF}{dl} = \frac{dF_w}{dl} + \frac{dF_m}{dl} + \frac{dF_l}{dl} + \frac{dF_b}{dl} \tag{2.1}$$

here, F represents the total disturbance of the manipulator when it moves underwater. F_w represents the water resistance; F_m represents the additional mass force; F_l represents the lift force and F_b represents the buoyancy force. Considering that the intelligent underwater manipulator has no airfoil structure, it is not necessary to consider the influence of lift, and only the other three items are considered. Therefore, the hydrodynamic factors are divided into three types, namely water resistance, additional mass force and equivalent gravity considering buoyancy. The dynamic equation of the manipulator can

be described as Eq (2.2):

$$\begin{cases} M(\theta)\ddot{\theta} + C(\theta,\dot{\theta})\dot{\theta} + G(\theta) + \tau_d(\theta,\dot{\theta}) = \tau, \\ M(\theta) = M_1(\theta) + M_2(\theta), \\ C(\theta,\dot{\theta}) = C_1(\theta,\dot{\theta}) + C_2(\theta,\dot{\theta}), \\ G(\theta) = G_1(\theta) - G_2(\theta) \end{cases} \tag{2.2}$$

here, $\theta, \dot{\theta}, \ddot{\theta}$ are the vectors of joint angle, angular velocity and angular acceleration of the two-joint manipulator respectively. $M_1(\theta)$ represents the acceleration inertia matrix of order $n \times n$ in joint space. $M_2(\theta)$ represents the additional mass force matrix. $C_1(\theta,\dot{\theta})$ represents the centripetal force and the coriolis force matrix. $C_2(\theta,\dot{\theta})$ is the water resistance matrices. $G_2(\theta)$ is the buoyancy matrices, and $G(\theta)$ is the equivalent gravity matrix considering the effect of buoyancy. $\tau_d(\theta,\dot{\theta})$ represents uncertainties, such as external disturbances. The right side of the equation τ represents the external torque matrix acting on the joints of the intelligent underwater manipulator.

According to the knowledge of fluid mechanics, the water resistance df_w of any unit in the underwater environment is given by Eq (2.3):

$$df_w = \frac{1}{2}\rho C_d D V(x)\|V(x)\|dx \tag{2.3}$$

The water resistance moment $d\tau_w$ is shown in Eq (2.4):

$$d\tau_w = \frac{1}{2}\rho C_d D \left(\begin{bmatrix} x & 0 & 0 \end{bmatrix}^T \cdot V(x) \right) \|V(x)\|dx \tag{2.4}$$

According to Morison's empirical equation, hydrodynamic unit dF, which contains the water resistance and additional mass forces, can be expressed as Eq (2.5):

$$dF = dFw + dFm = \frac{1}{2}\rho C_w D\|V(x)\|V(x)dx + \rho C_m A\frac{dV(x)}{dt}dx \tag{2.5}$$

At the same time, by integrating any element along the length of the connecting rod, the water resistance moment τ_w and the additional mass moment τ_m can be obtained, and their expressions are Eqs (2.6) and (2.7), respectively:

$$\tau_{wi} = \frac{1}{2}\rho C_w D_i \int_0^{l_i} \left(\begin{bmatrix} x_i & 0 & 0 \end{bmatrix}^T \cdot V_i(x) \right) |V_i(x)|\, dx, \quad i = 1, 2. \tag{2.6}$$

$$\tau_{mi} = \frac{\pi}{4}\rho C_m D_i^2 \int_0^{l_i} \left(\begin{bmatrix} x_i & 0 & 0 \end{bmatrix}^T \cdot \frac{dV_i(x)}{dt} \right) dx, \quad i = 1, 2. \tag{2.7}$$

here, ρ represents the fluid density, and D_i represents the diameter of the cylindrical rod, $l_i (i = 1, 2)$ represents the length of the two connecting rods, respectively. Because the manipulator structure is similar to the cylindrical structure, and approximate calculations can be made. $V_i(x)$ represents the velocity function, and A represents the projected area of the object in the direction perpendicular to the water flow velocity. C_w represents the water resistance coefficient, and C_m represents the additional mass force coefficient. In the actual analysis of dynamics, empirical values are often used for calculation, here $C_w = 1.0$ and $C_m = 1.0$ are taken into the calculation, respectively. The schematic diagram of the 2 -DOF manipulator motion model is shown in Figure 2.

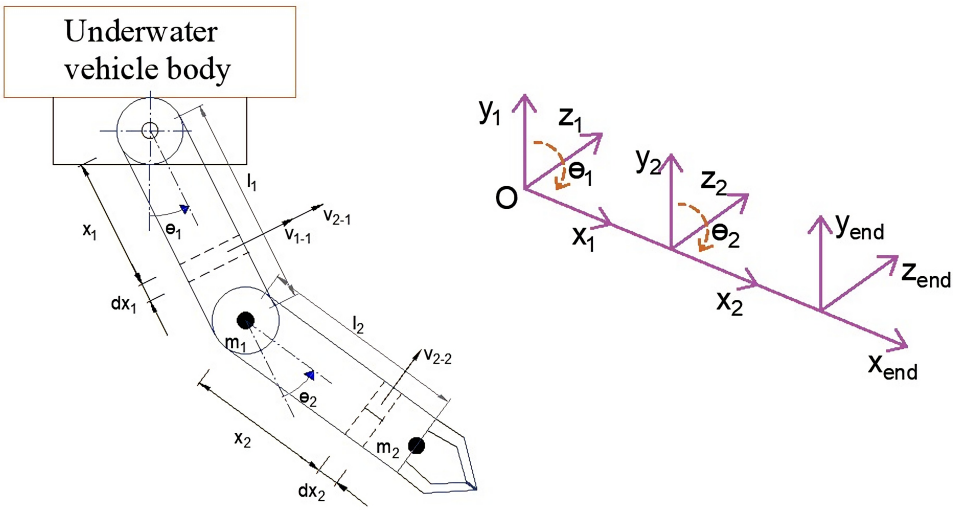

Figure 2. Schematic diagram of the motion model of the two-DOF manipulator.

In Figure 2, q_1 and q_2 denote the rotation angle of the two joints, respectively, dx_1 and dx_2 denote the unit length of the connecting rod, respectively, which are equal when they have been substituted into the calculation equations. v_{1-1} and v_{2-1} represent the normal velocities generated by the angular velocity of joint 1 and joint 2 to link 1 per unit length, respectively, while v_{2-2} denotes the normal velocity of the angular velocity of joint 2 on the connecting rod per unit length. These normal velocities have a direct influence on the generation of the hydrodynamic moment of the robotic linkage. A simple gripper is attached to the end of joint 2, which can be used for tasks such as underwater cable cutting. Based on Figure 2, multiple normal velocities can be calculated as Eqs (2.8)–(2.10), respectively:

$$v_{1-1} = x_1\dot{\theta}_1 \cos\theta_1, \tag{2.8}$$

$$v_{2-1} = x_1\dot{\theta}_1 \cos\theta_1 + \mathrm{x}_2\left(\dot{\theta}_1 + \dot{\theta}_2\right), \tag{2.9}$$

$$v_{2-2} = l_1\dot{\theta}_1 \cos\theta_2 + x_2\left(\dot{\theta}_1 + \dot{\theta}_2\right). \tag{2.10}$$

Substituting the above Eqs (2.8)–(2.10) into Eqs (2.6) and (2.7), the water resistance moments and additional mass moments for the two connecting rods can be calculated as Eqs (2.11)–(2.14), respectively:

$$\begin{aligned}\tau_{w1} =& \frac{1}{2}\rho C_w D_1 \int_0^{l_1} x_1\dot{\theta}_1 \cos\theta_1 \left|x_1\dot{\theta}_1 \cos\theta_1\right| x_1 dx \\ &+ \frac{1}{2}\rho C_w D_2 \int_0^{l_2} \left[x_1\dot{\theta}_1 \cos\theta_2 + \left(\dot{\theta}_1 + \dot{\theta}\right) x_2\right] \\ &\cdot \left|x_1\dot{\theta}_1 \cos\theta_2 + \left(\dot{\theta}_1 + \dot{\theta}_2\right) x_2\right| \cdot \left(l_1 \cos\theta_2 + x_2\right) dx,\end{aligned} \tag{2.11}$$

$$\begin{aligned}\tau_{m1} =& \frac{\pi}{4}\rho C_m D_1^2 \int_0^{l_1} \frac{d\left(x_1 \cdot \dot{\theta}_1 \cos\theta_1\right)}{dt} x_1 dx \\ &+ \frac{\pi}{4}\rho C_m D_2^2 \int_0^{l_2} \frac{d\left[x_1\dot{\theta}_1 \cos\theta_2 + x_2\left(\dot{\theta}_1 + \dot{\theta}_2\right) x_2\right]}{dt} \left(l_1 \cos\theta_2 + x_2\right) dx,\end{aligned} \tag{2.12}$$

$$\begin{aligned}\tau_{w2} =& \frac{1}{2}\rho C_w D_2 \int_0^{l_2} \left[x_1\dot{\theta}_1 \cos\theta_2 + x_2\left(\dot{\theta}_1 + \dot{\theta}_2\right)\right] \\ &\left|x_1\dot{\theta}_1 \cos\theta_2 + x_2\left(\dot{\theta}_1 + \dot{\theta}_2\right)\right| \cdot x_2 dx,\end{aligned} \tag{2.13}$$

$$\tau_{m2} = \frac{\pi}{4}\rho C_m D_2^2 \int_0^{l_2} \frac{d\left[x_1\dot{\theta}_1 \cos\theta_1 + x_2\left(\dot{\theta}_1 + \dot{\theta}_2\right)\right]}{dt} \cdot x_2 dx, \tag{2.14}$$

$$\tau_w = [\tau_{w1}, \tau_{w2}]^T = C_2\left[\dot{\theta}_1, \dot{\theta}_1\right]^T, \tag{2.15}$$

$$\tau_m = [\tau_{m1}, \tau_{m2}]^T = M_2\left[\ddot{\theta}_1, \ddot{\theta}_2\right]^T. \tag{2.16}$$

According to Eqs (2.15) and (2.16), the water resistance matrix C_2 and the additional mass force matrix M_2 can be obtained, respectively. The equivalent gravity matrix can be expressed as Eq (2.17):

$$G(\theta) = \left[m_1 g - \rho V_1 g, m_2 g - \rho V_2 g\right]^T = \left[m_1\left(1 - \rho/\rho_m\right), m_2\left(1 - \rho/\rho_m\right)\right]^T \tag{2.17}$$

here, V_1 and V_2 indicate the effective volume of the connecting rod, and ρ_m indicates the size of the density of the connecting rod.

3. Fuzzy logic sliding mode control algorithm for manipulator movement of underwater robot

In this section, when the underwater robot is in a hovering state, we approximately regard the base part connected to the manipulator as a fixed state, and do not consider the influence of the underwater robot body on the motion state of the manipulator.

3.1. Description of PID sliding mode control

In the state space of a general system, there is a sliding surface $s(t)$ that divides the state space of the system into two parts, namely $s(t) > 0$ and $s(t) < 0$. There are three cases of motion points on the sliding surface, as shown in Figure 3. Point A represents the normal point, the system movement point moves to the sliding surface $s(t) = 0$ and passes through point A. Point B represents the starting point, that is, the moving point reaches the sliding surface and leaves from point B to both sides. Point C represents the end point. When the moving point reaches the vicinity of the sliding surface, it tends to this point from both sides of the sliding surface. When all motion points in the system are termination points, the system reaches a steady state.

Therefore, for sliding mode control, the design of the sliding mode surface function $s(t)$ and the convergence control rate $\tau(t)$ are two important elements of the closed loop interval that allows the actual value to converge to the desired value.

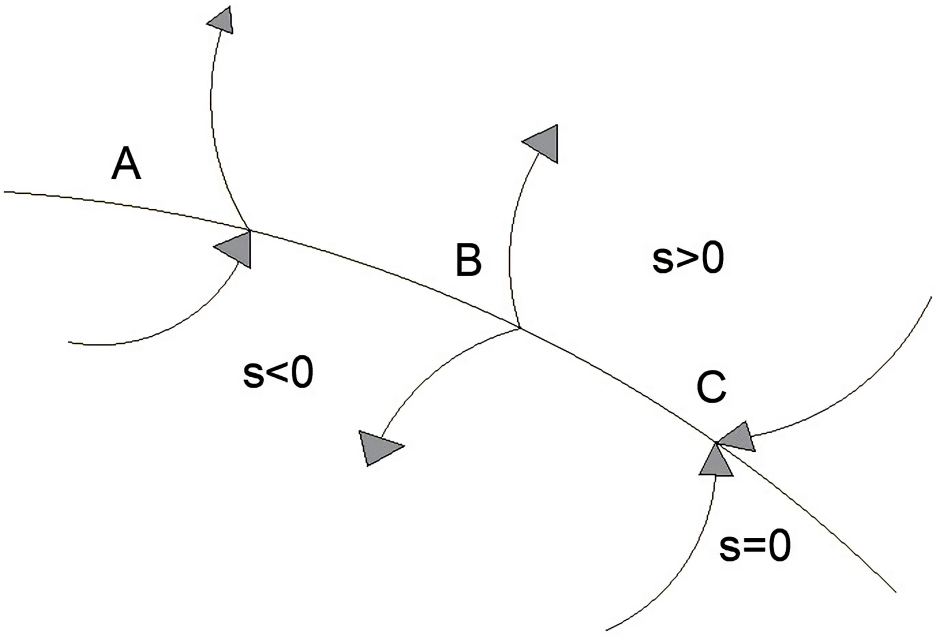

Figure 3. Characteristics of three points on sliding surface.

Based on Proportional-Integral-Differential (PID) control, the design of the sliding mode surface function $s(t)$ is described as Eqs (3.1) and (3.2), respectively:

$$s(t) = k_p e(t) + k_i \int e(t)dt + k_d \dot{e}(t), \tag{3.1}$$

$$e(t) = \theta_d(t) - \theta(t), \tag{3.2}$$

here k_p, k_i and k_d are the $n \times n$ order diagonal gain matrices and their expressions are $k_p = \text{diag}\left(k_{p1}, k_{p2}\right)$, $k_i = \text{diag}\left(k_{i1}, k_{i2}\right)$, and $k_d = \text{diag}\left(k_{d1}, k_{d2}\right)$, respectively.

The purpose of the sliding mode control is to move the tracking error $e(t)$ towards the sliding mode surface and eventually to the termination position. Therefore, a stable sliding surface is necessary, which can ensure that the error gradually approaches 0 with the increase of time. In Eq (3.2), $\theta_d(t)$ is the desired trajectory and $\theta(t)$ is the actual trajectory of the intelligent underwater manipulator joints.

It is well known that for systems with uncertainties and imposed disturbances, the complete full sliding mode control is generally a combination of equivalent control and switching control, and its expression is Eq (3.3):

$$\tau(t) = \tau_{eq}(t) + \tau_{sw}(t), \tag{3.3}$$

where $\tau(t)$ is the complete control law of sliding mode control. $\tau_{eq}(t)$ is the equivalent control law, which is usually designed for deterministic systems without external disturbances. $\tau_{sw}(t)$ is the switching control law, which can achieve robust control effects against uncertainties and external disturbances in the system.

Theorem 1. *If* $\Delta A_l \le |\Delta A| \le \Delta A_h$, $\Delta B_l \le |\Delta B| \le \Delta B_h$, *and* $\Delta C_l \le |\Delta C| \le \Delta C_h$, *and the following equation is satisfied:*

$$\begin{aligned}\tau_{sw}(t) = \operatorname{sgn}(s(t)) \cdot [k_d(C+\Delta C)]^{-1} \cdot \\ \left\{ \left[\left|\Delta_h - A^{-1}C\Delta C_l\right| |\dot{\theta}| + \left|\Delta B_h - B^{-1}C\Delta C_l\right| |G(\theta)| \right.\right. \\ \left.\left. + k_d|m(t)|\right] - \left|C^{-1}\Delta C_h\right| \left(k_p|\dot{e}| + k_i|e| + k_d|\ddot{\theta}|\right) \right\}\end{aligned} \tag{3.4}$$

Then, one can obtain that the following control equation system is stable:

$$s(t) = k_p e(t) + k_i \int e(t)dt + k_d\dot{e}(t), \tag{3.5}$$

$$e(t) = \theta_d(t) - \theta(t). \tag{3.6}$$

Proof. From Eq (3.2), one can get Eq (3.7):

$$\ddot{\theta}(t) = -M^{-1}(\theta)C(\theta,\dot{\theta})\dot{\theta} - M^{-1}(\theta)G(\theta) - M^{-1}(\theta)\tau_d(\theta,\dot{\theta}) + M^{-1}(\theta)\tau(t). \tag{3.7}$$

Considering the uncertain factors existing in the system, Eq (3.7) can be described as Eq (3.8):

$$\ddot{\theta}(t) = -(\mathrm{A} + \Delta\mathrm{A})\dot{\theta} - (\mathrm{B} + \Delta B)G(\theta) + (\mathrm{C} + \Delta C)\tau(t) - m(t) \tag{3.8}$$

here, $A = M^{-1}(\theta)C(\theta,\dot{\theta})$, $B = C = M^{-1}(\theta)$, and $m(t) = M^{-1}(\theta)\tau_d(\theta,\dot{\theta})$ represent external disturbances, respectively. At the same time, ΔA, ΔB and ΔC are considered the uncertain factors existing in the system, and it is specified that the uncertain factors have a range, that is $\Delta A_l \le |\Delta A| \le \Delta A_h$, $\Delta B_l \le |\Delta B| \le \Delta B_h$, and $\Delta C_l \le |\Delta C| \le \Delta C_h$. l and h represent the lower and upper limits of the uncertain factors, respectively.

A further simplification of Eq (3.8) is given as Eq (3.9):

$$\begin{aligned}\ddot{\theta}(t) &= -(\mathrm{A} + \Delta\mathrm{A})\dot{\theta} - (\mathrm{B} + \Delta B)G + (\mathrm{C} + \Delta C)\tau(t) - m(t) \\ &= -\mathrm{A}\dot{\theta} - \mathrm{B}G + \mathrm{C}\tau(t) - \Delta\mathrm{A}\dot{\theta} - \Delta BG + \Delta C\tau(t) - m(t) \\ &= -\mathrm{A}\dot{\theta} - \mathrm{B}G + \mathrm{C}\tau(t) - N(t)\end{aligned} \tag{3.9}$$

where $N(t) = \Delta\mathrm{A}\dot{\theta} + \Delta BG - \Delta C\tau(t) + m(t)$.

From Eq (3.1), it follows that:

$$\begin{aligned}\dot{s}(t) &= k_p\dot{e}(t) + k_i e(t) + k_d\ddot{e}(t) \\ &= k_p\dot{e}(t) + k_i e(t) + k_d\left[\ddot{\theta}_d + (A+\Delta A)\dot{\theta}\right. \\ &\quad \left. + (B+\Delta B)G(\theta) - (C+\Delta C)\tau(t) + m(t)\right]\end{aligned} \tag{3.10}$$

If the uncertainties and external disturbance factors in the system are not considered, it can be deduced that $\Delta A = \Delta B = \Delta C = m(t) = 0$. Simplifying the Eq (3.10) as the following Eq (3.11):

$$\dot{s}(t) = k_p\dot{e}(t) + k_i e(t) + k_d\left[\ddot{\theta}_d + A\dot{\theta} + BG(\theta) - C\tau(t)\right] \tag{3.11}$$

The equivalent control $\tau_{eq}(t)$ expression can be taken as the following Eq (3.12):

$$\tau_{eq}(t) = (k_d C)^{-1}\left[k_p\dot{e} + k_i e + k_d\left(\ddot{\theta}_d + A\dot{\theta} + BG(\theta)\right)\right] \tag{3.12}$$

However, if there are undesired disturbances in the control system in the form of parameter changes, and load disturbances, etc., then we need to perform supplementary control, that is, switching control, which can perform robust stability control against these uncertain disturbances. In order to verify the stability of the system, according to the Lyapunov function theory, the Lyapunov function is proposed to be described as the following Eq (3.13):

$$V(t) = \frac{1}{2} s^T(t) s(t) \tag{3.13}$$

In the case of a stable system, $\dot{V}(t) = s^T(t)\dot{s}(t) < 0$, $s(t) \neq 0$ should be guaranteed. Wherein, in the full control law $\tau(t) = \tau_{eq}(t) + \tau_{sw}(t)$, in order to satisfy the system stability condition, the first order derivative of $V(t)$ is expressed as the following Eq (3.14):

$$\begin{aligned} \dot{V}(t) =& s^T \dot{s} \\ =& s^T \left\{ k_p \dot{e} + k_i e + k_d \left[\ddot{\theta}_d + (A + \Delta A)\dot{\theta} + (B + \Delta B) G(\theta) \right.\right. \\ & \left.\left. -(C + \Delta C) \left(\tau_{eq}(t) + \tau_{sw}(t) + m(t) \right) \right] \right\} \\ =& s^T \left\{ k_p \dot{e} + k_i e + k_d \left[\ddot{\theta}_d + (A + \Delta A)\dot{\theta} + (B + \Delta B) G(\theta) + m(t) \right\} \right. \\ & - s^T k_d (C + \Delta C) \left((k_d C)^{-1} \left[k_p \dot{e} + k_i e + k_d \left(\ddot{\theta}_d + \right. \right. \right. \\ & \left. \left. \left. A\dot{\theta} + BG(\theta) \right) \right] + \tau_{sw}(t) \right] \end{aligned} \tag{3.14}$$

Continuing to simplify Eq (3.14), one can obtain the following Eq (3.15):

$$\begin{aligned} \dot{V}(t) =& s^T k_p \left[\left(\Delta A - A^{-1} C \Delta C \right) \dot{\theta} + \left(\Delta B - B^{-1} C \Delta C \right) G(\theta) + m(t) \right] \\ & - C^{-1} \Delta C \left(k_p \dot{e} + k_i e + k_d \ddot{\theta} \right) - s^T k_d (C + \Delta C) \tau_{sw}(t) \\ =& s^T k_p \left[\left| \Delta A - A^{-1} C \Delta C \right| |\dot{\theta}| + \left| \Delta B - B^{-1} C \Delta C \right| |G(\theta)| + |m(t)| \right] \\ & - \left| C^{-1} \Delta C \right| \left(k_p |\dot{e}| + k_i |e| + k_d |\ddot{\theta}| \right) - s^T k_d (C + \Delta C) \tau_{sw}(t) \end{aligned} \tag{3.15}$$

Based on the Eq (3.15), the switching control law $\tau_{sw}(t)$ can be designed as the following Eq (3.16):

$$\begin{aligned} \tau_{sw}(t) = & \operatorname{sgn}(s(t)) \cdot [k_d (C + \Delta C)]^{-1} \cdot \\ & \left\{ \left[\left| \Delta_h - A^{-1} C \Delta C_l \right| |\dot{\theta}| + \left| \Delta B_h - B^{-1} C \Delta C_l \right| |G(\theta)| \right. \right. \\ & \left. \left. + k_d |m(t)| \right] - \left| C^{-1} \Delta C_h \right| \left(k_p |\dot{e}| + k_i |e| + k_d |\ddot{\theta}| \right) \right\} \end{aligned} \tag{3.16}$$

Substituting Eq (3.16) into Eq (3.15), one can deduce the first order derivative of the Lyapunov function $\dot{V}(t) < 0$, $s(t) \neq 0$, which proves the stability of the system. □

Next, an expression for the switching control law in conventional sliding mode control is given by the following Eq (3.17):

$$\tau_{sw}(t) = \varepsilon_{sw} \cdot \operatorname{sgn}(s(t)) \tag{3.17}$$

where $\varepsilon_{sw} = \operatorname{diag}(\varepsilon_{sw1}, \varepsilon_{sv2} \ldots \varepsilon_{svn})$ denotes the switching control gain with an uncertain upper bound, and the switching control is designed in the form of the symbolic function $\operatorname{sgn}(s(t))$ in Eq (3.17).

As can be seen from the expression for the switching control law in conventional sliding mode control, the state switching process of the sign function contained in the Eq (3.17) is not smooth, which will lead to an undesired control trajectory, and eventually the control trajectory will appear chattering. The physical explanation can be described as follows: when the trajectory of the system reaches the switching surface, its velocity is finite and its own inertia causes the point of motion to cross the sliding mode surface $s = 0$, thus eventually creating a chattering phenomenon.

3.2. The proposition of fuzzy logic sliding mode control model

In this study, in order to improve the chattering defect of traditional sliding mode control, combined with fuzzy logic control method, a Fuzzy-logic Sliding Mode Control (FSMC) model based on fuzzy logic control is designed to improve the defect of sliding mode control.

As a control method different from the traditional control theory, the FSMC method gives full play to its advantages of not needing a mathematical model of the object and having robustness in the control effect, and shows its advantages in the control field with relevant characteristics. In some complex systems, especially when the system has imprecise and uncertain information, the effect of fuzzy logic control is often better than that of conventional control methods.

For conventional sliding mode control, the addition of fuzzy logic control methods can smooth out the control signal and reduce or avoid the jittering phenomenon in the conventional sliding mode control process. Based on the traditional control method, this study proposes an improved fuzzy logic sliding mode control method. For the fuzzy logic control system, the inputs include the sliding mode surface function $s(t)$ and its first order derivative $\dot{s}(t)$, and the system output switches the control law $\tau_{sw}(t)$, whose output is essentially a part of the input torque of the intelligent underwater manipulator joint. The overall control block diagram is shown in Figure 4. The switching control law for the proposed control method can be expressed as the following equation:

$$\tau_{sw}(t) = \varepsilon_f \cdot \tau_f(t) \tag{3.18}$$

where ε_f is the normalized term of the system output, and $\tau_f(t)$ is the resultant output of the fuzzy logic sliding mode control system under the action of inputs $s(t)$ and $\dot{s}(t)$.

In a fuzzy logic sliding mode control system, the rules for the input control parameters s, $\dot{s}$ and the output control parameter τ_f are shown in Figure 5(a)–(c). Figure 5(d) shows the input and output of the fuzzy inference system in a spatial view.

Table 1. Fuzzy rule table based on two inputs single output.

τ_f ($\dot{s}$ / s)	*NB*	*NS*	*ZO*	*PS*	*PB*
PB	ZO	PS	PB	PB	PB
PS	NM	ZO	PS	PB	PB
ZO	NB	NS	ZO	PS	PB
NS	NB	NS	NS	ZO	PS
NB	NB	NB	NB	NS	ZO

Table 1 describes the fuzzy rule table for the control system. The fuzzy sets are defined as PB = positive large; PS = positive small; ZO = zero; NS = negative small; NB = negative large. Each input is divided into 5 intervals, and finally multiple fuzzy rules are generated. Usually, the input parameters in the fuzzy system are also called fuzzy variables, and the Gaussian membership function of normal distribution is selected here.

When the fuzzy rule of design is in the mth item, it can be expressed as follows:

$$\text{IF } s \text{ is } A^m \text{ and } \dot{s} \text{ is } B^m, \text{ THEN } \tau_f \text{ is } C^m$$

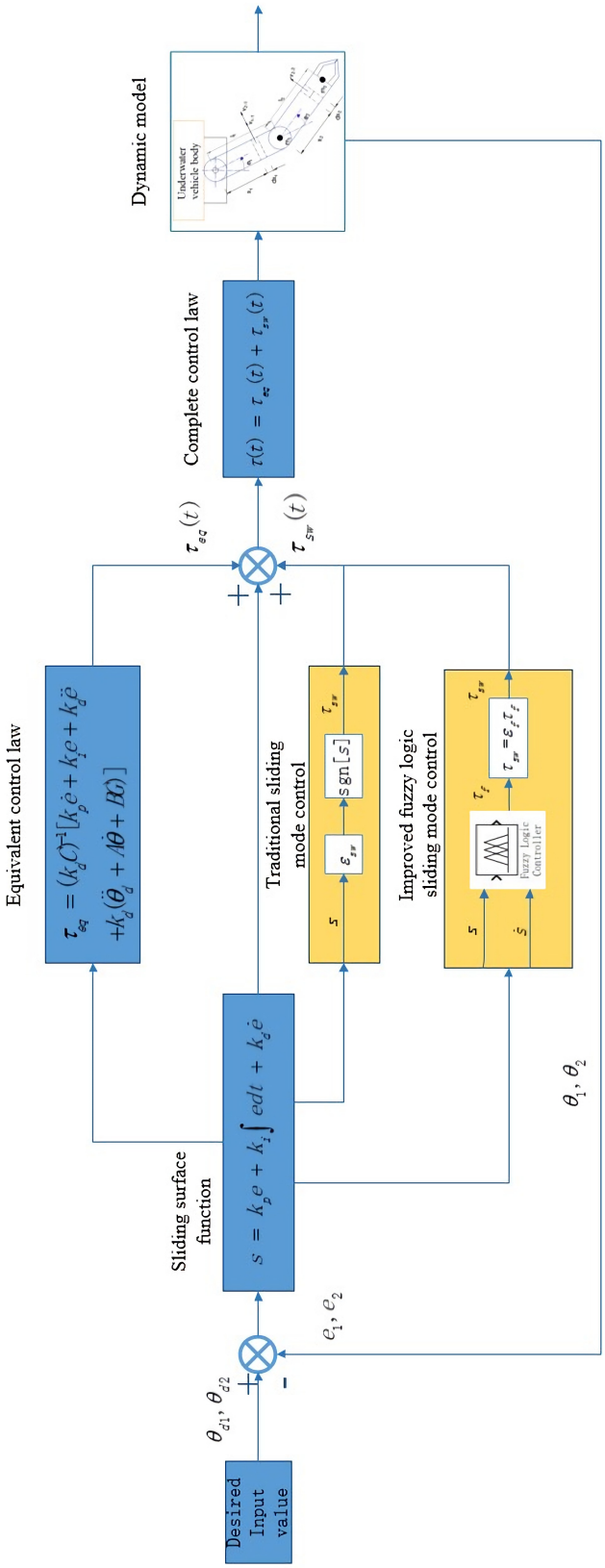

Figure 4. Block diagram of the controller.

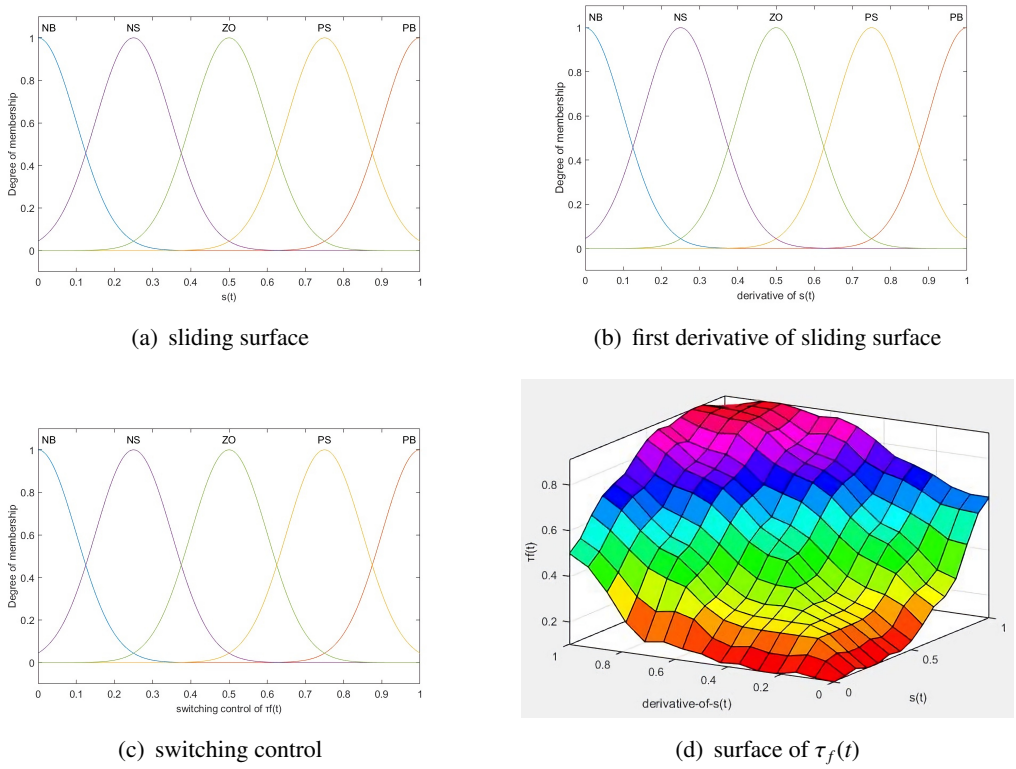

(a) sliding surface

(b) first derivative of sliding surface

(c) switching control

(d) surface of $\tau_f(t)$

Figure 5. FSMC control parameters.

here A^m and B^m represent the input rule base, C^m denotes the output rule base, $m = 1, 2, \ldots$ n, and n denotes the number of fuzzy rules in the control system.

At the same time, the output of the fuzzy system is also made accurate by using the centre of gravity averaging method in the process of anti-fuzzification. The final full control law based on the FSMC control method is expressed as Eq (3.19):

$$\tau(t) = \tau_{eq}(t) + \tau_{sw}(t) = \tau_{eq}(t) + \varepsilon_f \cdot \tau_f(t) \tag{3.19}$$

Theorem 2. *IF s is A^m and $\dot{s}$ is B^m, THEN τ_f is C^m, $\varepsilon_f > k_d|N(t)|$, and the following equation is satisfied:*

$$\begin{aligned} \dot{V}(t) &= s^T \left[-\varepsilon_f \tau_f(t) + k_d N(t)\right] \\ &= -\varepsilon_f \left|s^T\right| \left|\tau_f(t)\right| + k_d \left|s^T\right| |N(t)| \\ &= \left[-\varepsilon_f + k_d|N(t)|\right] \left|s^T\right|, \end{aligned} \tag{3.20}$$

here, ε_f is the normalized term of the system output, and $\tau_f(t)$ is the resultant output of the fuzzy logic sliding mode control system under the action of inputs $s(t)$ and $\dot{s}(t)$. Then, one can obtain that the following control equation system is stable:

$$\tau(t) = \tau_{eq}(t) + \tau_{sw}(t) = \tau_{eq}(t) + \varepsilon_f \cdot \tau_f(t) \tag{3.21}$$

Proof. In order to prove the stability of the proposed system, similarly, based on the classical Lyapunov function theory, the proposed Lyapunov function is described as Eq (3.22):

$$V(t) = \frac{1}{2} s^T(t) s(t), \ \ s(t) \neq 0 \tag{3.22}$$

Calculating the first order derivative of Eq (3.22), and substituting Eq (3.9) into (3.22), one gets the following Eq (3.23):

$$\begin{aligned}\dot{V}(t) =& s^T \left\{k_p\dot{e} + k_i e + k_d \left[\ddot{\theta}_d - \ddot{\theta}\right]\right\} \\ =& s^T \left\{k_p\dot{e} + k_i e + k_d \left[\ddot{\theta}_d + (A + \Delta A)\dot{\theta} + (B + \Delta B)G\right.\right. \\ & \left.\left. -(C + \Delta C)\left(\tau_{eq}(t) + \tau_{sw}(t) + m(t)\right]\right\} \\ =& s^T \left\{k_p\dot{e} + k_i e + k_d \left[\ddot{\theta}_d + A\dot{\theta} + BG - C\left(\tau_{eq}(t) + \tau_{sw}(t)\right) + \mathrm{N}(t)\right\}\right. \\ =& - s^T k_d(C + \Delta C)\left((k_d C)^{-1}\left[k_p\dot{e} + k_i e + k_d\left(\ddot{\theta}_d + \right.\right.\right. \\ & \left.\left.\left. A\dot{\theta} + BG(\theta))\right] + \tau_{sw}(t)\right]\end{aligned} \tag{3.23}$$

Substituting the expression for $\tau_{eq}(t)$ into Eq (3.23), one can obtain the simplification of Eq (3.24):

$$\begin{aligned}\dot{V}(t) =& s^T \left\{k_p\dot{e} + k_i e + k_d\left(\ddot{\theta}_d + A\dot{\theta} + BG\right)\right. \\ & - k_d C\left[(k_d C)^{-1}\left(k_p\dot{e} + k_i e + k_d\left(\ddot{\theta}_d\right.\right.\right. \\ & \left.\left.\left. + A\dot{\theta} + BG)\right) + \tau_{sw}(t)\right] + k_d N(t)\Big\} \\ =& s^T\left[-\tau_{sw}(t) + k_d N(t)\right] \\ =& s^T\left[-\varepsilon_f \tau_f(t) + k_d N(t)\right]\end{aligned} \tag{3.24}$$

Considering that the output fuzzy set in the fuzzy system is normalized in the interval [0, 1], it can be deduced that:

$$\begin{cases} \left|\tau_f(t)\right| \le 1, \\ \left|s^T(t)\right|\left|\tau_f(t)\right| \le \left|s^T(t)\right|. \end{cases} \tag{3.25}$$

The result of combining Eqs (3.24) and (3.25) can be described as the following Eq (3.26):

$$\begin{aligned}\dot{V}(t) =& \; s^T\left[-\varepsilon_f \tau_f(t) + k_d N(t)\right] \\ =& -\varepsilon_f\left|s^T\|\tau_f(t)\right| + k_d\left|s^T\right||N(t)| \\ =& \left[-\varepsilon_f + k_d|N(t)|\right]\left|s^T\right|\end{aligned} \tag{3.26}$$

It is easy to see from Eq (3.26) that if the value of ε_f is chosen to be larger than the value of $k_d|N(t)|$, then it can be concluded that $\dot{V}(t) < 0$, which proves the asymptotic stability of the control system. It is guaranteed that the error in the control process of the system converges to the sliding mode surface. □

4. Simulation results

When the underwater robot is in the hovering state, the joints of the manipulator at the bottom are unfolded, and the manipulator structure is shown in Figure 2. In order to simulate the underwater environment and the accurate model, it is assumed that the mass of the connecting rod of the intelligent underwater manipulator is concentrated at the end position, which is marked m_1 and m_2 in Figure 2. The parameters of the intelligent underwater manipulator are shown in Table 2.

4.1. Hydrodynamic numerical analysis and quantitative research of underwater manipulator

The effects of complex disturbing factors in the underwater environment are taken into account, especially in terms of the effects of fluid mechanics. It is necessary to investigate the kinematic

Table 2. Parameters of Two-DOF manipulator.

Manipulator	*Quality*(*kg*)	*Length*(*m*)	$Cross-sectionalarea(\mathrm{cm}^2)$
Joint 1	1.50	0.40	19.64
Joint 2	1.50	0.40	19.64

effects, simulation and modeling of the hydrodynamics of a two-DOF intelligent underwater manipulator. Meanwhile, the parametric equations of the dynamic model of the manipulator are deduced in detail in the second section of this study. All simulations are done with MATLAB/Simulink tools in this study. The work on the numerical analysis and quantitative study of the hydrodynamics of the intelligent underwater manipulator will provide a good basis for the reduction of simulation errors and the accuracy of the model.

In order to conduct a comparative study, at the same time, we consider the influence of three external disturbance effects(water resistance moment, additional mass moment, buoyancy) on the trajectory of the intelligent underwater manipulator. The degree of their influence on the actual trajectory is studied through simulation analysis. The desired trajectories of the two joints during the simulation are $\theta_{d1} = 2\sin(3t) + 3\cos(t)$, and $\theta_{d2} = -\sin(2t) - 2\cos(t)$, respectively.

Figure 6 shows the trajectory of the intelligent underwater manipulator under the combined influence of both the water resistance moment and the additional mass moment. As shown in the Figure 6, under the condition of water resistance and additional mass force, the trajectory deviation of the intelligent underwater manipulator continues to increase. It can be known that the manipulator is more affected by water resistance and additional mass force when it moves in the underwater environment.

Meanwhile, as shown in Figure 7, the trajectory control of the intelligent underwater manipulator when the effect of buoyancy is considered. The simulation results show the strong influence of hydrodynamic factors on the trajectory of the underwater environment. It can be seen from the Figure 7 that at the beginning there are large errors in the trajectory of the manipulator in both cases. However, with the increase of time, the trajectory of the intelligent underwater manipulator under the influence of buoyancy begins to fit the expected trajectory after about $1s$, and the trajectory is well tracked. The deviation in the trajectory of the manipulator under water resistance and additional mass forces continues to increase. It can be seen that the manipulator is more influenced by water resistance and additional mass forces when moving in a submerged environment.

In summary, it has been demonstrated that attenuating or counteracting the effects of hydrodynamic forces is necessary to control the trajectory of the manipulator in underwater operations.

4.2. Simulation of FSMC for underwater manipulator

In a real underwater environment, the intelligent underwater manipulator is controlled to track the trajectory based on the set trajectory information, and the accuracy of the control directly affects the accuracy of the actual operation. The desired motion trajectory equation in the simulation is set as $\theta_{d1} = \theta_{d2} = 3\cos(t) + 2\sin(2t)$, $0 \le t \le 10s$. Moreover, in the sliding mode surface equation based on PID control design, the parameters are chosen as $k_p = \mathrm{diag}(50, 50)$, $k_i = \mathrm{diag}(20, 20)$, and $k_d = \mathrm{diag}(5, 5)$. For the SMC method, the control gain parameter is chosen as $\varepsilon_{sw} = \mathrm{diag}(3500, 2500)$. Similarly, for the FSMC method, the gain parameter is designed to be $\varepsilon_f = \mathrm{diag}(1000, 750)$ in the simulation.

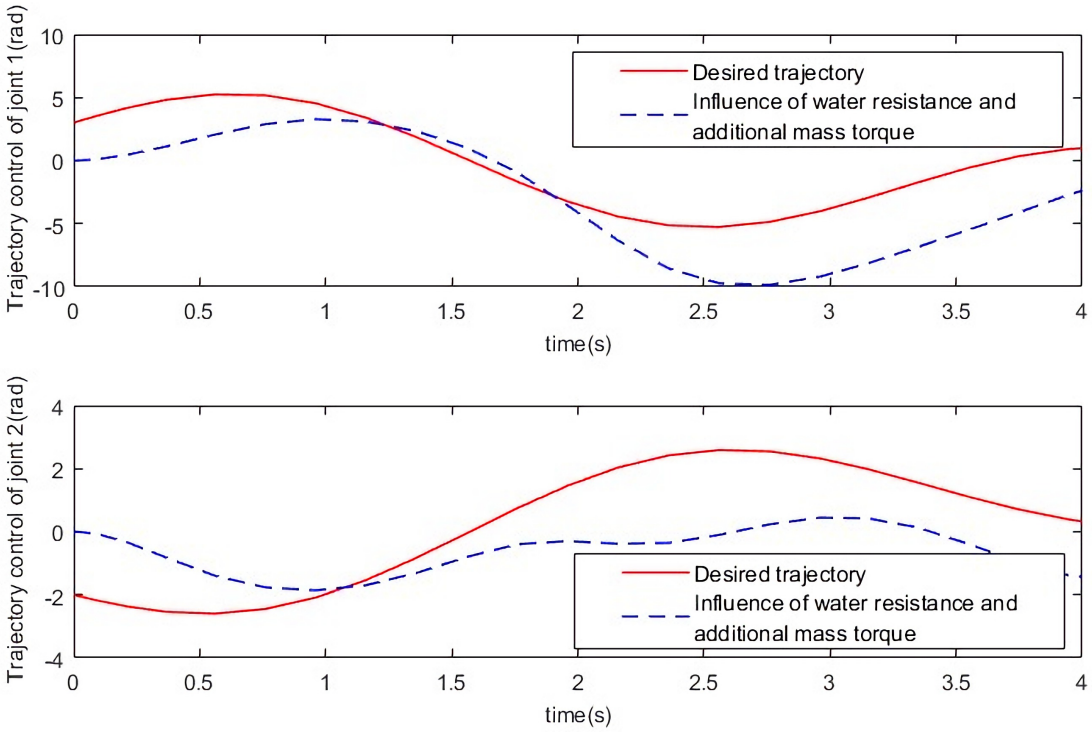

Figure 6. The effects of the water resistance and additional mass torque.

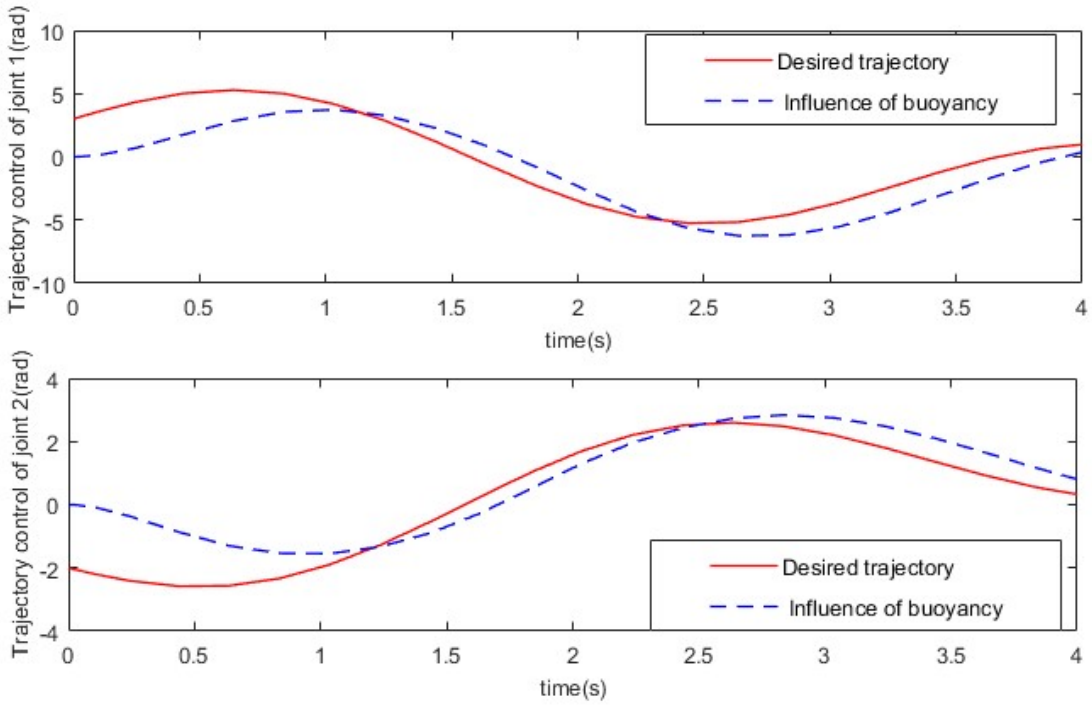

Figure 7. The effects of the buoyancy torque.

In order to demonstrate the superiority of the control method proposed in this study, FSMC is compared with the traditional sliding mode control method, and the trajectory tracking of the intelligent underwater manipulator is simulated and verified.

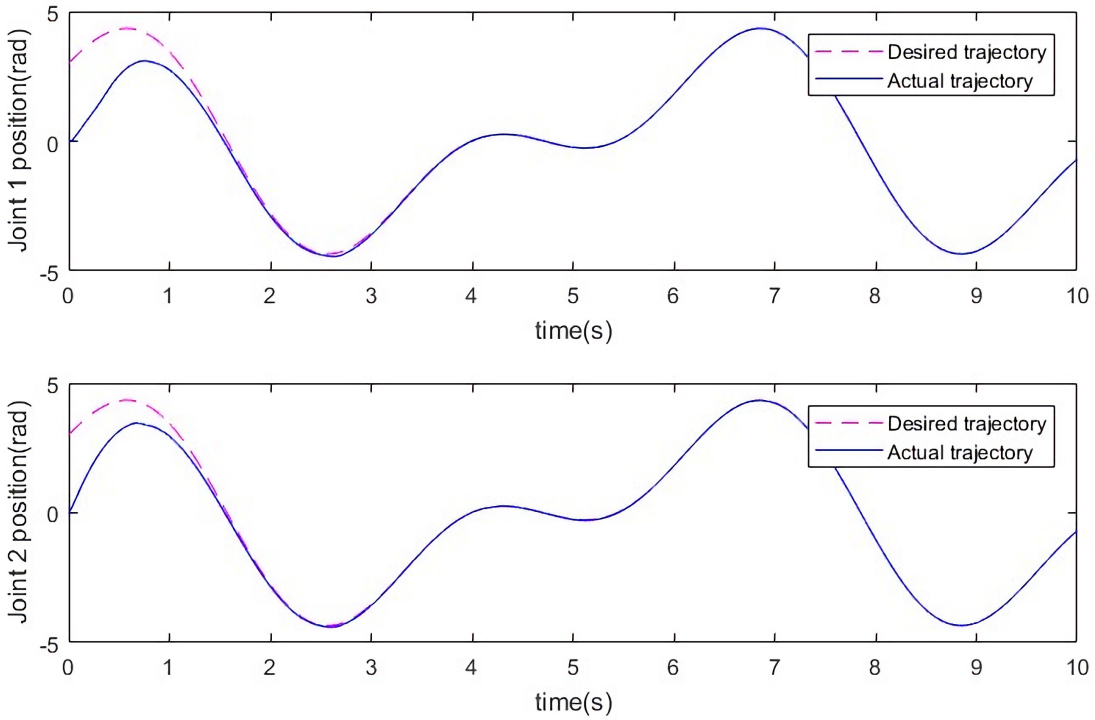

Figure 8. Actual trajectory tracking performances of SMC.

Under the traditional sliding mode control method, the actual and desired trajectory tracking effect of the two joints of the intelligent underwater manipulator are shown in Figure 8, and the angular velocity tracking actual and desired trajectory of the two joints of the intelligent underwater manipulator are shown in Figure 9, respectively.

Similarly, under the fuzzy logic sliding mode control method, the actual and desired trajectory tracking effect of the two joints of the intelligent underwater manipulator are shown in Figure 10, and the angular velocity tracking actual and desired trajectory of the two joints of the intelligent underwater manipulator are shown in Figure 11, respectively.

It can be seen from Figures 8–11 that in the simulation comparison between the FSMC method proposed in this study and the traditional SMC method, the joint trajectory tracking effect based on the FSMC method is better.

As can be seen from Figures 8–11, the FSMC-based method has a better trajectory tracking effect in the simulation comparison between the proposed FSMC method and the conventional SMC method. In the figures, the joint 1 of intelligent underwater manipulator only has a partial deviation from the start of the simulation to 1.5s. With the extension of the simulation time, the trajectory convergence achieves the expected effect. The trajectory convergence time of joint 2 of the intelligent underwater manipulator is shorter and faster, and some small-scale errors caused by trajectory tracking are acceptable.

As shown in Figures 12 and 13, the comparisons of the trajectory tracking errors corresponding to

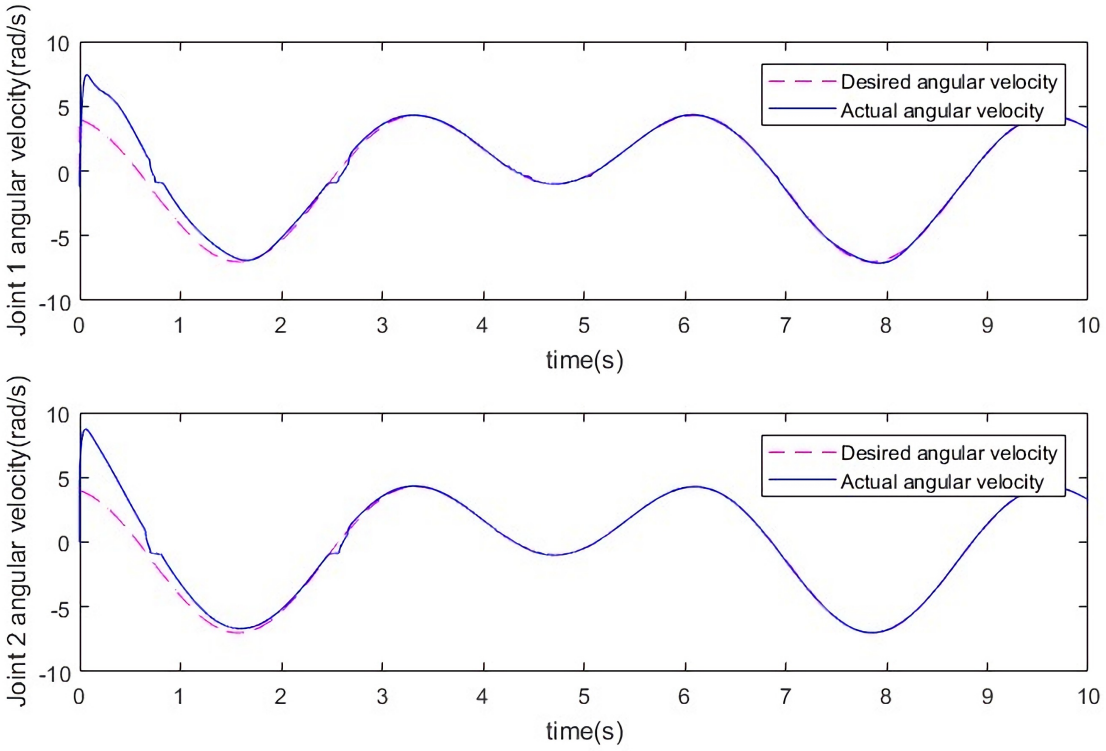

Figure 9. Actual angular velocity tracking performances of SMC.

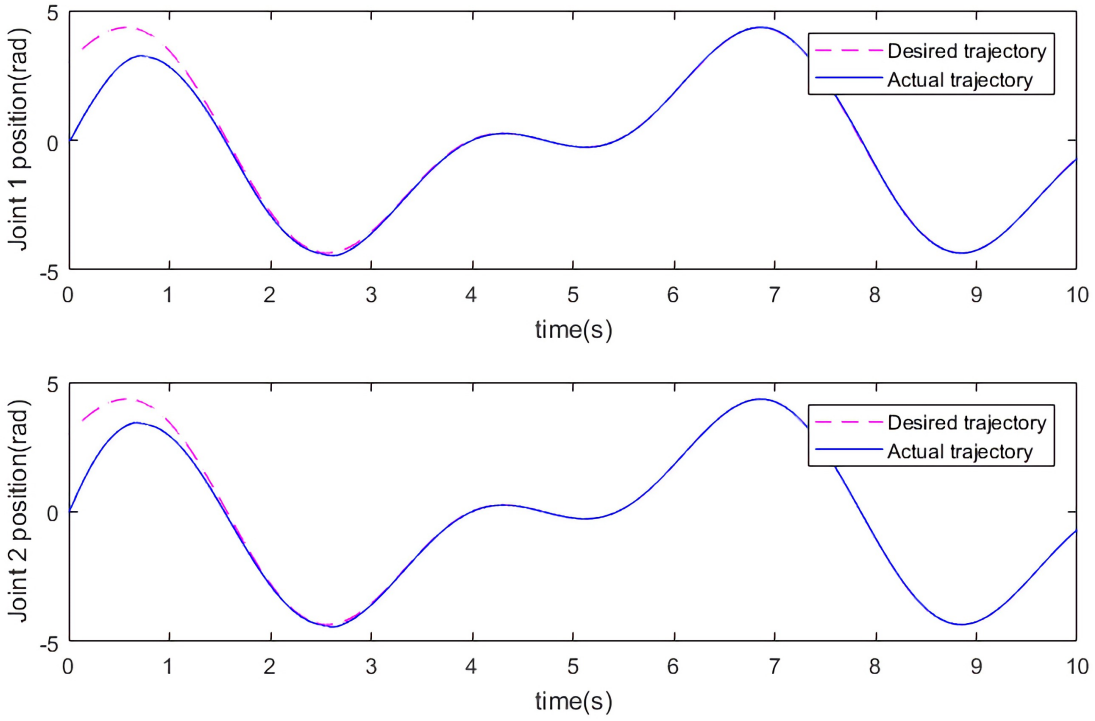

Figure 10. Tracking performances of FSMC.

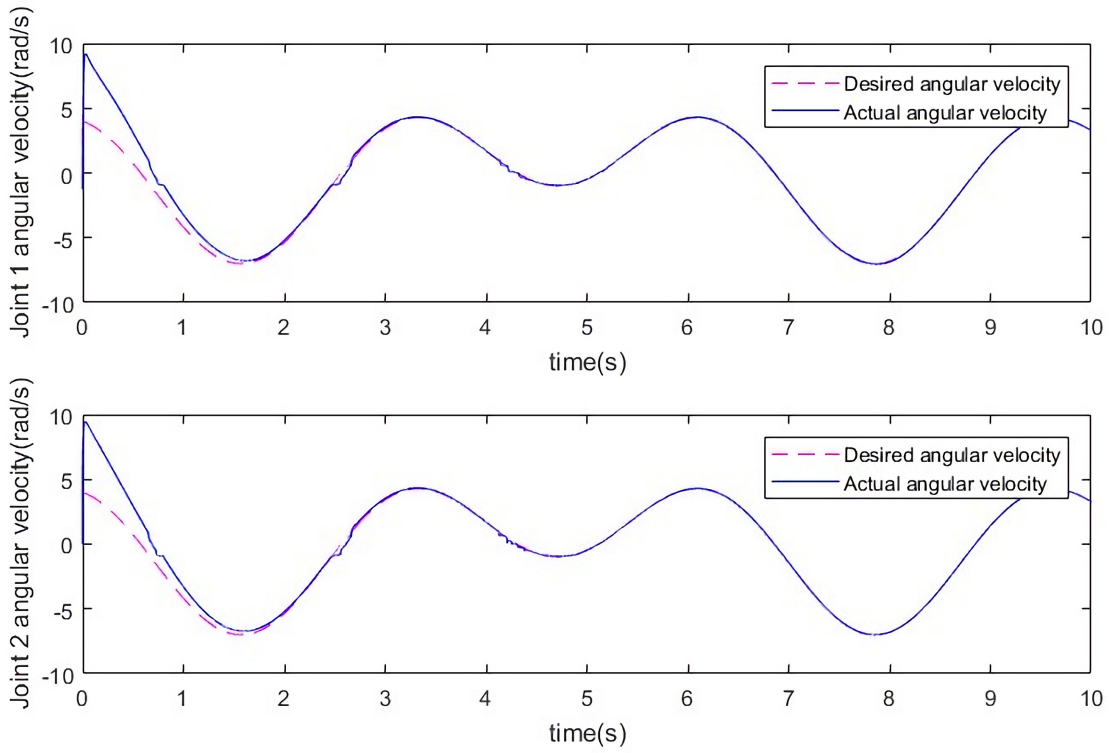

Figure 11. Tracking performances of FSMC.

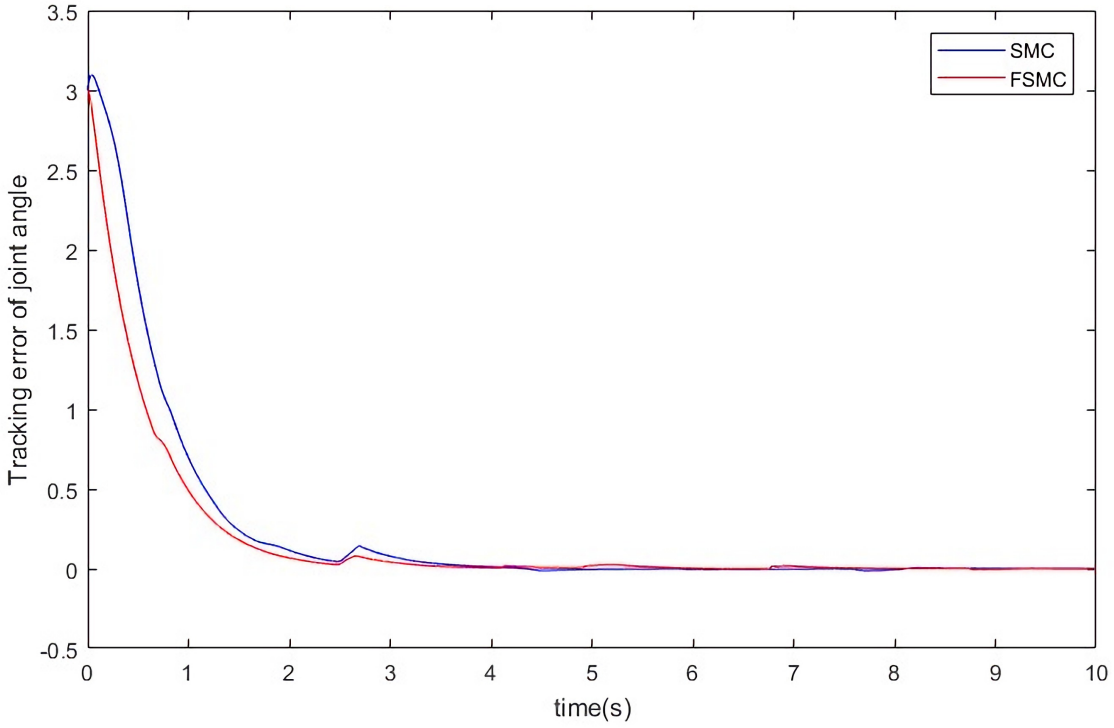

Figure 12. Tracking error of joint 1.

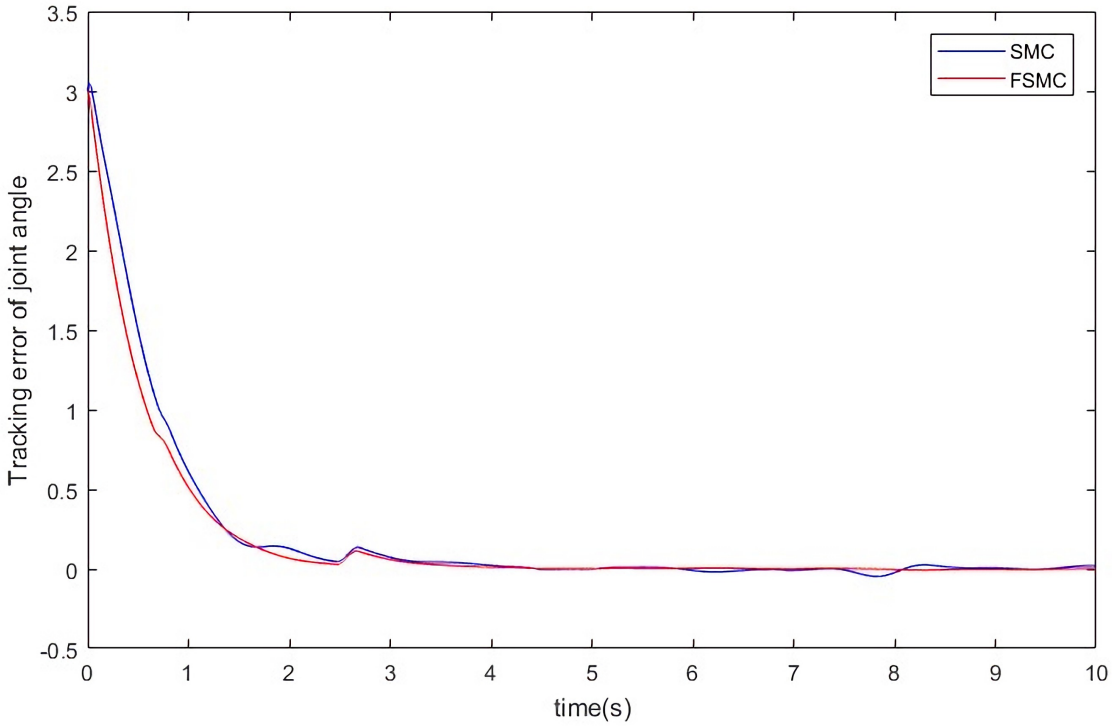

Figure 13. Tracking error of joint 2.

the two joints of the intelligent underwater manipulator under the comparison of the two control methods are described, respectively. These control effects are generated under the action of the two different control methods, e.g., SMC and FSMC. Figure 12 describes the tracking error of the joint 1 on intelligent underwater manipulator, Figure 13 describes the tracking error of the joint 2 on intelligent underwater manipulator. They describe the detailed comparison of the trajectory tracking errors corresponding to the two joints of the intelligent underwater manipulator. From the figures, the superiority of the trajectory tracking of the FSMC method can be more clearly observed. The traditional sliding mode control method has a big defect, which will produce an obvious chattering phenomenon during trajectory tracking, which is unacceptable for the actual intelligent underwater manipulator motion control. Therefore, combined with fuzzy logic control, a new fuzzy logic sliding mode control method is proposed in this study. The new control method improves the chattering phenomenon to a great extent and makes the input of joint torque smoother.

Figures 14 and 15 are the joint torque input curves of the intelligent underwater manipulator based on the SMC and FSMC methods, respectively. It can be clearly seen from Figures 14 and 15 that the joint input process based on the FSMC method is smooth and gentle. In contrast, the joint input based on the SMC method suffers from a large chattering problem, which can seriously affect the stability and reliability of the control system. Therefore, it is finally verified and proved by simulation that the proposed new method has good tracking effect on the desired trajectory, small tracking error, short convergence time, and improves the joint input defect problem of the traditional control method.

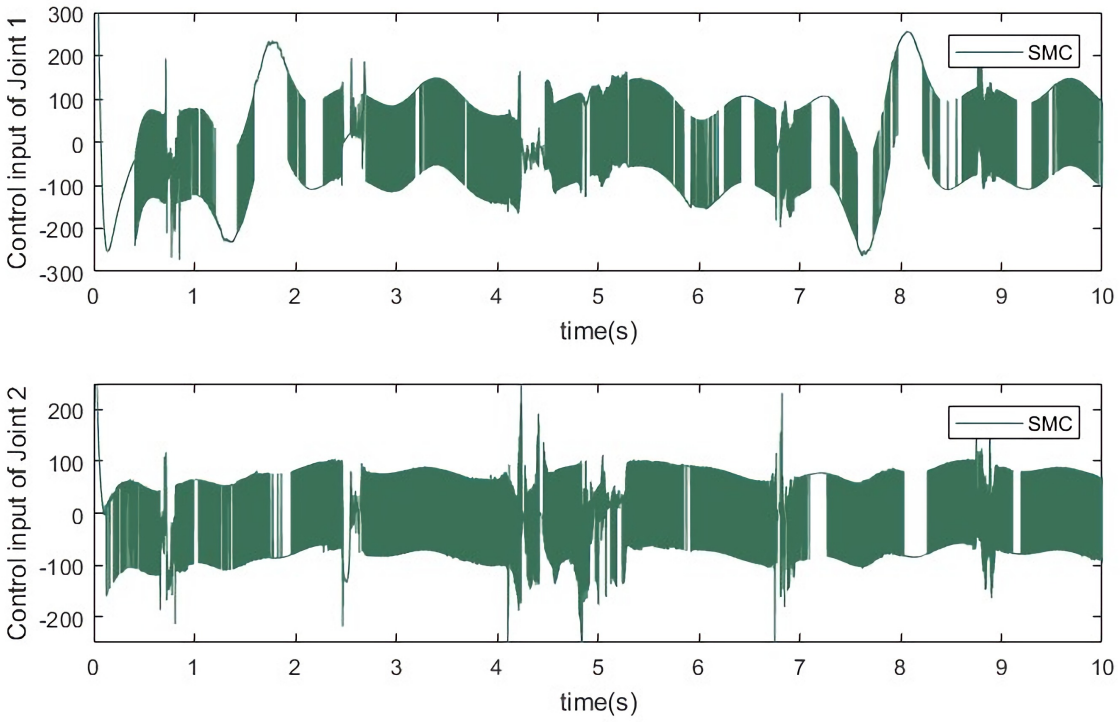

Figure 14. Joint control input based on SMC.

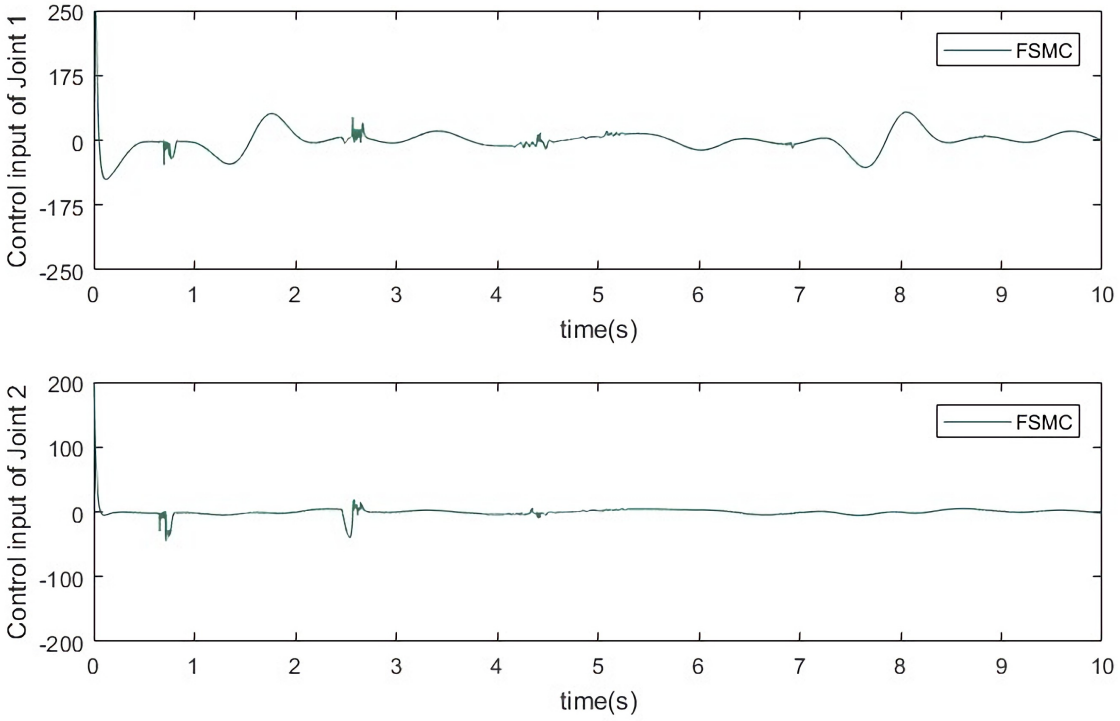

Figure 15. Joint control input based on FSMC.

5. Conclusions

In this study, based on the two-link intelligent underwater manipulator model, combined with the Lagrangian equation and Morison equation, an accurate dynamic model of the manipulator in the underwater environment is established. On the basis of the sliding mode surface of the PID structure, considering the uncertainty and external disturbance of the system, the equivalent control law and switching control law of the sliding mode control are analyzed and studied. Aiming at the large trajectory tracking error and chattering of control input existing in the traditional SMC method, a new FSMC method is proposed. In order to demonstrate the superiority of the new method proposed in this study, a simulation comparison was made with the traditional sliding mode control algorithm. The simulation results show that the proposed FSMC method can effectively eliminate the tracking error and external disturbance factors in the trajectory control process of the intelligent underwater manipulator. Furthermore, the instability problem of the control input of the traditional control method is largely improved.

Future research topics of interest include study on the stable and precise control of the intelligent underwater manipulator under complex dynamic disturbance conditions, and it can also be based on the traditional sliding mode control to further improve the fuzzy control system to achieve a more accurate and stable control effect of the intelligent underwater manipulator.

Use of AI tools declaration

The authors declare they have not used Artificial Intelligence (AI) tools in the creation of this article.

Acknowledgment

This work was supported by the Wuhan University of Science and Technology International Talent Fund Project (grant number 2023J0501 and grant number 2023J0503).

Conflict of Interest

The authors declare there is no conflict of interest.

References

1. J. Meng, B. Zhang, T. Wei, X. He, X. Li, Robust finite-time stability of nonlinear systems involving hybrid impulses with application to sliding-mode control, *Math. Biosci. Eng.*, **20** (2023), 4198–4218. https://doi.org/10.3934/mbe.2023196
2. X. Shao, Z. Liu, B. Jiang, Sliding-mode controller synthesis of robotic manipulator based on a new modified reaching law, *Math. Biosci. Eng.*, **19** (2022), 6362–6378. https://doi.org/10.3934/mbe.2022298
3. H. Huang, G. Tang, H. Chen, J. Wang, L. Han, D. Xie, Vibration suppression trajectory planning of underwater flexible manipulators based on incremental kriging-assisted optimization algorithm, *J. Marine Sci. Eng.*, **11** (2023), 938. https://doi.org/10.22214/ijraset.2023.49958

4. X. Zheng, Q. Tian, Q. Zhang, Development and control of an innovative underwater vehicle manipulator system, *J. Marine Sci. Eng.*, **11** (2023), 548. https://doi.org/10.3390/jmse11030548

5. M. Khadembashi, H. Moeenfard, Beyond pull-in angle control of a dual axis torsional micro-actuator considering bending effects, *Appl. Math. Modelling*, **107** (2022), 133–150. https://doi.org/10.1016/j.apm.2022.02.016

6. G. Jing, L. Lei, Y. Gang, Dynamic modeling and experimental analysis of an underwater glider in the ocean, *Appl. Math. Modelling*, **108** (2022), 392–407. https://doi.org/10.1016/j.apm.2022.03.034

7. C. Paredis, H. B. Brown, P. K. Khosla, A rapidly deployable manipulator system, *Rob. Auton. Syst.*, **21** (1997), 289–304. https://doi.org/10.1016/S0921-8890(97)00081-X

8. S. Zhou, C. Shen, Y. Xia, Z. Chen, S. Zhu, Adaptive robust control design for underwater multi-DoF hydraulic manipulator, *Ocean Eng.*, **248** (2022), 110822. https://doi.org/10.1016/j.oceaneng.2022.110822

9. J. Long, Y. Tian, W. Chen, J. Leng, Y. Wang, Locating, trajectory planning and control of an underwater propeller cleaning manipulator, *Ocean Eng.*, **243** (2022), 110262. https://doi.org/10.1016/j.oceaneng.2021.110262

10. B. Ema, A. Osr, A. Db, B. Xz, Comprehensive modeling and identification of nonlinear joint dynamics for collaborative industrial robot manipulators, *Control Eng. Pract.*, **101** (2020). https://doi.org/10.1016/j.conengprac.2020.104512

11. Z. Chen, X. Yang, X. Liu, Rbfnn-based nonsingular fast terminal sliding mode control for robotic manipulators including actuator dynamics, *Neurocomputing*, **362** (2019), 72–82. https://doi.org/10.12816/0061297

12. V. Muralidharan, T. K. Mamidi, S. Guptasarma, A. Nag, S. Bandyopadhyay, A comparative study of the configuration-space and actuator-space formulations of the lagrangian dynamics of parallel manipulators and the effects of kinematic singularities on these, *Mech. Mach. Theory*, **130** (2018), 403–434. https://doi.org/10.1016/j.mechmachtheory.2018.07.009

13. H. Abdellatif, B. Heimann, Computational efficient inverse dynamics of 6-dof fully parallel manipulators by using the lagrangian formalism, *Mech. Mach. Theory*, **44** (2009), 192–207. https://doi.org/10.1016/j.mechmachtheory.2008.02.003

14. I. Carlucho, D. W. Stephens, C. Barbalata, An adaptive data-driven controller for underwater manipulators with variable payload, *Appl. Ocean Res.*, **113** (2021), 102726. https://doi.org/10.1016/j.apor.2021.102726

15. P. S. Londhe, S. Mohan, B. M. Patre, L. M. Waghmare, Robust task-space control of an autonomous underwater vehicle-manipulator system by pid-like fuzzy control scheme with disturbance estimator, *Ocean Eng.*, **139** (2017), 1–13. https://doi.org/10.1016/j.oceaneng.2017.04.030

16. G. Q. Zeng, X. Q. Xie, M. R. Chen, J. Weng, Adaptive population extremal optimization-based pid neural network for multivariable nonlinear control systems, *Swarm Evolut. Comput.*, **44** (2018). https://doi.org/10.1016/j.swevo.2018.04.008

17. H. Farivarnejad, S. Moosavian, Multiple impedance control for object manipulation by a dual arm underwater vehicle?manipulator system, *Ocean Eng.*, **89** (2014), 82–98. https://doi.org/10.1016/j.oceaneng.2014.06.032

18. G. Zhong, C. Wang, W. Dou, Fuzzy adaptive pid fast terminal sliding mode controller for a redundant manipulator, *Mech. Syst. Signal Proc.* **159** (2021), 107577. https://doi.org/10.1016/j.ymssp.2020.107577

19. Z. Yuguang, Y. Fan, Dynamic modeling and adaptive fuzzy sliding mode control for multi-link underwater manipulators, *Ocean Eng.*, **187** (2019), 106202. https://doi.org/10.1016/j.oceaneng.2019.106202

20. J. Lin, R. J. Lian, Stability indices for a self-organizing fuzzy controlled robot: A case study, *Eng. Appl. Artif. Intell.*, **23** (2010), 1019–1034. https://doi.org/10.1016/j.engappai.2010.04.005

21. A. F. Amer, E. A. Sallam, W. M. Elawady, Adaptive fuzzy sliding mode control using supervisory fuzzy control for 3 dof planar robot manipulators, *Appl. Soft Comput.*, **11** (2011), 4943–4953. https://doi.org/10.1016/j.asoc.2011.06.005

22. K. Lu, W. Zhou, G. Zeng, Y. Zheng, Constrained population extremal optimization-based robust load frequency control of multi-area interconnected power system, *Int. J. Electr. Power Energy Syst.*, **105** (2019), 249–271. https://doi.org/10.1016/j.ijepes.2018.08.043

23. H. Nejatbakhsh Esfahani, V. Azimirad, M. Danesh, A time delay controller included terminal sliding mode and fuzzy gain tuning for underwater vehicle-manipulator systems, *Ocean Eng.*, **107** (2015), 97–107. https://doi.org/10.1016/j.oceaneng.2015.07.043

24. F. Maurelli, S. Krupiński, X. Xiang, Y. Petillot, AUV localisation: a review of passive and active techniques, *Int. J. Intell. Rob. Appl.*, 2021.

25. H. Huang, Q. Tang, J. Li, W. Zhang, X. Bao, H. Zhu, et al., A review on underwater autonomous environmental perception and target grasp, the challenge of robotic organism capture, *Ocean Eng.*, **195** (2020), 106644. https://doi.org/10.1016/j.oceaneng.2019.106644

26. F. Maurelli, M. Carreras, J. Salvi, D. Lane, K. Kyriakopoulos, G. Karras, et al., The PANDORA project: A success story in AUV autonomy, in *OCEANS 2016 - Shanghai*, (2016), 1–8. https://doi.org/10.1109/OCEANSAP.2016.7485618

27. X. Xiao, S. Joshi, Process planning for five-axis support free additive manufacturing, *Addit. Manuf.*, **36** (2020), 101569. https://doi.org/10.1016/j.addma.2020.101569

28. X. Xiao, B. M. Roh, F. Zhu, Strength enhancement in fused filament fabrication via the isotropy toolpath, *Appl. Sci.*, **11** (2021), 6100. https://doi.org/10.3390/app11136100

29. X. Xiao, S. Joshi, J. Cecil, Critical assessment of shape retrieval tools (srts), *Int. J. Adv. Manuf. Technol.*, **116** (2021), 3431–3446. https://doi.org/10.1002/ece3.7285

30. N. Wang, Y. Zhang, C. K. Ahn, Q. Xu, Autonomous pilot of unmanned surface vehicles: Bridging path planning and tracking, *IEEE Trans. Veh. Technol.*, **71** (2022), 2358–2374. https://doi.org/10.1109/TVT.2021.3136670

31. N. Wang, T. Chen, X. Kong, Y. Chen, R. Wang, Y. Gong, et al., Underwater attentional generative adversarial networks for image enhancement, *IEEE Trans. Human Mach. Syst.*, **53** (2023), 490–500. https://doi.org/10.1109/THMS.2023.3261341

32. N. Wang, Y. Gao, H. Zhao, C. K. Ahn, Reinforcement learning-based optimal tracking control of an unknown unmanned surface vehicle, *IEEE Trans. Neural Networks Learn. Syst.*, **32** (2021), 3034–3045. https://doi.org/10.1109/TNNLS.2020.3009214

AIMS Press